

2006

Double Resonance Spectroscopy of the $B^{\prime}\bar{B} 1\Sigma_u^+$ State of H_2

R. C. Ekey

A. Marks

Elizabeth McCormack

Bryn Mawr College, emccorma@brynmawr.edu

[Let us know how access to this document benefits you.](#)

Follow this and additional works at: http://repository.brynmawr.edu/physics_pubs

 Part of the [Physics Commons](#)

Custom Citation

R.C. Ekey, A. Marks and E.F. McCormack, *Phys. Rev. A* **73**, 23412 (2006).

This paper is posted at Scholarship, Research, and Creative Work at Bryn Mawr College. http://repository.brynmawr.edu/physics_pubs/28

For more information, please contact repository@brynmawr.edu.

Double resonance spectroscopy of the $B''\bar{B} \ ^1\Sigma_u^+$ state of H_2

R. C. Ekey, Jr., A. Marks, and E. F. McCormack
 Bryn Mawr College, Bryn Mawr, Pennsylvania 19010, USA
 (Received 28 September 2005; published 14 February 2006)

Double resonance spectroscopy via the $EF \ ^1\Sigma_g^+, \nu'_{EF}=6, J'$ state has been used to probe the rovibrational structure of the *ungerade* double-well $B''\bar{B} \ ^1\Sigma_u^+$ state of H_2 . Transitions to the $B''\bar{B} \ ^1\Sigma_u^+, \nu_{\bar{B}}=17-35, J=0-4$ levels of the outer-well and to the $\nu_{B''\bar{B}}=46-50, J=0-4$ levels of the combined inner and outer wells above the barrier have been recorded by detecting both molecular and atomic ion production as a function of energy by using a time of flight mass spectrometer. Theoretical energy calculations incorporating the most recent potential curves have been used to aid in the assignment of observed transitions. Over 70 new rovibrational term energies are reported. Where comparisons are possible, good agreement is observed between the experimental measurements reported here and those of previous measurements. While significant perturbations are observed in the energy region above the double-well barrier, assignments to states with dominant inner and outer-well characteristics can still be made. Distinct dynamical behaviors of the levels below, at, and above the barrier have also been observed.

DOI: [10.1103/PhysRevA.73.023412](https://doi.org/10.1103/PhysRevA.73.023412)

PACS number(s): 33.80.Rv, 33.80.Eh, 33.20.Ni

I. INTRODUCTION

The hydrogen molecule, being the simplest stable neutral molecule, is an important system for probing fundamental quantum-mechanical effects in molecules. The structure of its energy levels continues to provide an important test of *ab initio* methods used to accurately account for deviations from the Born-Oppenheimer approximation in molecular systems. Double-well states in H_2 are formed by an avoided crossing at relatively small internuclear separation between a bound state and a doubly excited dissociative state and, at large internuclear separation, by a crossing with the ion-pair configuration. The result is an electronic state consisting of an inner and outer-well separated by a potential energy barrier. Such states are of interest because of their unusual structure and stable configuration at large internuclear spacings. While the double well states in the *gerade* manifold of H_2 , have been extensively studied [1–3], those in the *ungerade* manifold have not [4–7].

The $B''\bar{B}, 3 \ ^1\Sigma_u^+$ state of H_2 is the third member of the *ungerade* series of double-well states in H_2 . It is associated with the third dissociation threshold at large internuclear separation R and levels with $\nu_{B''\bar{B}} > 10$, lie above the ionization threshold leading to a potentially rich competition in decay dynamics. With its large internuclear separation ($R > 7$ a.u.) levels of the $\bar{B} \ ^1\Sigma_u^+$ outer well are difficult to observe due to poor vibrational wavefunction overlap with the ground state. While predicted by Dabrowski and Herzberg over 30 years ago [4], it was not until recently that the outer-well levels were observed experimentally by de Lange *et al.* [6]. To access the outer-well states they used a triple resonance excitation scheme via the $B \ ^1\Sigma_u^+$ and $I' \ ^1\Pi_u$ states in H_2 . They observed transitions to the $\nu_{\bar{B}}=21-35, J=0, 2$, and 4 outer-well levels located below the barrier.

To further explore the rovibrational structure of the *ungerade* double-well $B''\bar{B} \ ^1\Sigma_u^+$ state, we have used double resonance spectroscopy through the $J'=0-3$ rotational levels of

the $EF \ ^1\Sigma_g^+, \nu'_{EF}=6$ state. The double resonance technique allows the observation of transitions from individually selected rotational levels of the intermediate $EF \ ^1\Sigma_g^+, \nu'_{EF}=6$ state, thereby greatly reducing spectral congestion. This relatively simple two-color excitation scheme also results in significant signals due to good vibrational wave function overlap between the $EF \ ^1\Sigma_g^+, \nu'_{EF}=6$ state and the $B''\bar{B} \ ^1\Sigma_u^+$ state. Spectra were recorded by using a time of flight mass spectrometer gated to detect both molecular and atomic ion production. As discussed below, transitions to Rydberg levels were generally observed in only the molecular ion detection channel, while transitions to the $B''\bar{B} \ ^1\Sigma_u^+$ state were observed in both, thus this dual detection capability aided us in making transition assignments. Over 100 levels of the $B''\bar{B} \ ^1\Sigma_u^+$ state have been observed, more than 70 of which are reported and assigned for the first time. Energy calculations using the best available potential energy curves [7] were used to aid in the assignment of levels. As the energy approaches and surpasses the barrier, the accuracy of the calculated energies deteriorates significantly, indicating that the results presented here may be valuable for fine-tuning the potential energy curve of the $B''\bar{B} \ ^1\Sigma_u^+$ state. Where comparisons are possible, good agreement is observed between the experimental measurements reported here and those of previous measurements [6].

In what follows we present first a description of the experimental approach and the apparatus used. Double resonance spectra are then presented and the resulting term energies and their uncertainties are reported. Throughout, levels of the ground state are labeled by double primes, levels of the intermediate $EF \ ^1\Sigma_g^+$ state are labeled by single primes, and levels of the $B''\bar{B} \ ^1\Sigma_u^+$ state are identified by an absence of primes. Two vibrational level numbering schemes are in use for the $B''\bar{B} \ ^1\Sigma_u^+$ state. In one, $\nu_{B''\bar{B}}$ refers to a sequential vibrational numbering of all vibrational levels in the double-well. In the other $\nu_{\bar{B}}$ refers to a sequential vibrational numbering of the outer-well states only. Given there are ten bound states in the inner well, these two numbering schemes

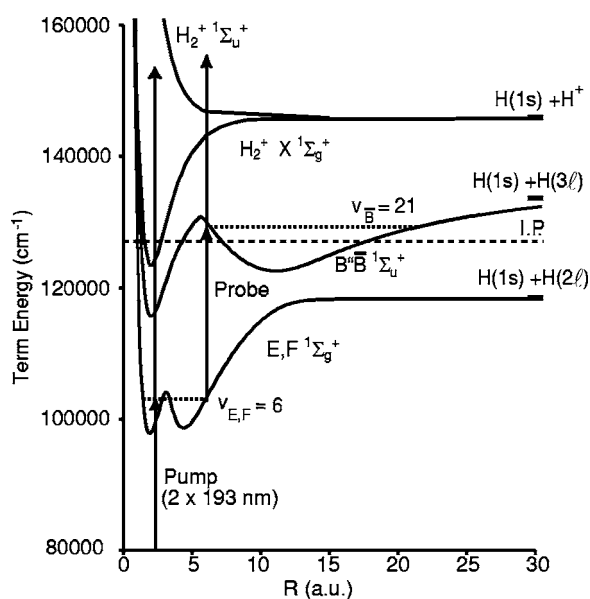


FIG. 1. Excitation scheme and adiabatic potential energy curves of the relevant states of H_2 and H_2^+ .

result in vibrational level numbers that differ by ten for states above the barrier.

II. EXPERIMENT

The two-color, resonantly enhanced multiphoton ionization scheme used to access rovibrational levels of the outer and combined well of the $B''\bar{B}^1\Sigma_u^+$ state is shown in Fig. 1. Two pulsed Nd:YAG-pumped dye lasers were used as the pump and probe lasers. The pump laser tuned near 193 nm was used to excite the two-photon $EF^1\Sigma_g^+, \nu'_{EF}=6, J'=0-3 \leftarrow X^1\Sigma_g^+, \nu''=0, J''=0-3$ transitions, and the probe laser was used to excite single photon transitions from the $EF^1\Sigma_g^+, \nu'_{E,F}=6, J'$ state to the $\nu_{\bar{B}}=17-35, J=0-4$ rovibrational levels of the outer well and to the combined inner and outer well $\nu_{B''\bar{B}}=46-50, J=0-4$ levels above the barrier of the $B''\bar{B}^1\Sigma_u^+$ state.

Figure 2 shows a schematic of the experimental arrangement. Pump light at 193 nm was generated by sum-frequency mixing in BBO the fourth harmonic of Nd:YAG laser light at 266 nm with the output of a dye laser operating at ~ 705 nm. Probe light was generated by using a second Nd:YAG-pumped dye laser in the wavelength range of 415–375 nm. To access states in the 375–350 nm wavelength range, the probe light at 750–700 nm was frequency doubled in BBO.

Pump pulses with 100–200 μJ of energy were focused by a 25-cm-focal-length lens into the interaction region. The focal position of this lens was displaced by ~ 1 cm to maximize the ratio of the one and two-color ion signals. This arrangement helped to minimize $EF^1\Sigma_g^+$ state depletion effects in the line shapes of the observed probe transitions. The probe light was collimated into a beam with a diameter of ~ 3 mm and sent into the interaction region unfocused. Probe pulse energies could be varied from 3 mJ to 50 μJ by using

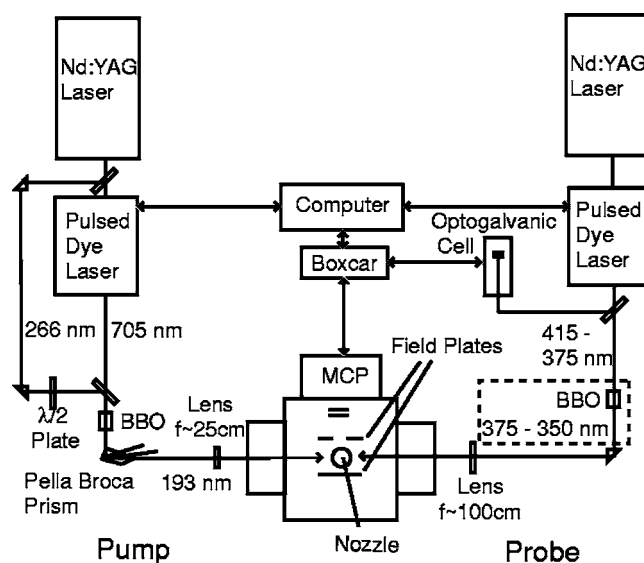


FIG. 2. Schematic of the experimental arrangement.

neutral density filters placed in the probe beam.

A portion of the probe beam was sent to a hollow-cathode Uranium lamp with Argon as a buffer gas. The optogalvanic effect in these two elements along with Iron was used to calibrate the probe laser wavelength [8,9]. Most transition energies are estimated to be accurate to ~ 0.20 cm^{-1} , with the dominant source of uncertainty arising from wavelength nonlinearities in the drive of the probe laser. The bandwidth of the probe-laser beam was between ~ 0.07 and ~ 0.15 cm^{-1} depending on wavelength.

A collision-free beam of molecular hydrogen was produced by using a supersonic expansion of pure H_2 from a solenoid-driven pulsed valve. Counter-propagating pump and probe light pulses crossed the molecular beam in the interaction region located between two electric field plates. A time delay of 40 ns was introduced between the pump and probe pulses to distinguish ions produced by the pump beam alone and those produced by two-color resonant excitation. Ions generated by the two-color process were accelerated into the time-of flight mass spectrometer by a pulsed electric field of 125 V/cm. Probe spectra were acquired by fixing the frequency of the pump light and scanning the frequency of the probe light. While scanning the frequency of the probe light, the production of H_2^+ and H^+ ions was monitored by using a boxcar integrator.

III. RESULTS AND DISCUSSION

Probe spectra of transitions to the outer well, $B''\bar{B}^1\Sigma_u^+, \nu_{\bar{B}}=17-35, J=0-4$ levels and to the $B''\bar{B}^1\Sigma_u^+, \nu_{B''\bar{B}}=46-50, J=0-4$ levels above the barrier were recorded by using the $Q(0), Q(1), Q(2),$ and $Q(3)$ branches of the $EF^1\Sigma_g^+, \nu'_{EF}=6 \leftarrow X^1\Sigma_g^+, \nu''=0$ pump transition. Term energies were obtained by adding the probe transition energies to the $EF^1\Sigma_g^+, \nu'_{E,F}=6, J'$ term energies obtained by adding the rotational intervals of Dieke [10], accurate to a few times 0.01 cm^{-1} , to the $E, F^1\Sigma_g^+, \nu'_{E,F}=6, J'=0$ term energy of

TABLE I. Experimental term energies and assignments for observed outer-well levels of the $B''\bar{B}^1\Sigma_u^+$ state located below the double-well barrier. Provided for comparison are the differences Δ^a between the current measurements and those of de Lange *et al.* [6] for $J=0, 2$, and 4. Energy values are in cm^{-1} .

$\nu_{B''\bar{B}}$	$\nu_{\bar{B}}$	$J=0$	Δ^a	$J=1$	$J=2$	Δ^a	$J=3$	$J=4$	Δ^a
24	17	127719.28(20)		127720.99(20)	127724.62(20)				
25	18	127947.07(20)		127948.96(20)	127952.26(20)		127957.69(23)	127964.51(26)	
26	19	128169.40(20)		128171.24(20)	128174.54(20)		128181.06(20)	128186.68(20)	
27									
28	20	128385.98(20)		128387.48(20)	128390.92(21)		128396.21(20)	128402.51(20)	
29	21	128597.27(20)	0.26	128598.78(20)	128602.44(20)	0.08	128607.34(20)	128614.35(20)	0.01
30	22	128803.30(20)	-0.11	128805.48(27)	128808.29(20)	-0.32	128813.59(20)	128819.81(34)	-0.49
31	23	129004.30(22)	0.02	129005.97(22)	129009.18(20)	-0.05	129014.43(20)	129020.61(20)	-0.17
32	24	129199.94(20)	-0.29	129201.77(20)	129204.98(20)	-0.17	129210.01(27)	129216.73(20)	0.10
33	25	129391.18(20)	-0.19	129392.90(20)	129396.15(20)	-0.09	129401.09(20)	129407.52(22)	-0.02
34									
35	26	129577.60(20)	-0.24	129579.23(31)	129582.42(20)	-0.20	129587.47(20)	129593.83(20)	0.06
36	27	129759.89(20)	0.24	129761.30(31)	129764.51(20)	0.10	129769.06(20)	129775.54(20)	0.02
37	28	129937.02(20)	-0.08	129937.99(20)	129941.79(20)	0.04	129945.92(20)	129952.63(20)	-0.07
38	29	130110.12(20)	0.00	130111.71(21)	130114.69(20)	-0.06	130119.30(20)	130125.41(30)	-0.14
39	30	130278.50(20)	-0.06	130280.84(22)	130283.54(23)	-0.07	130288.49(20)	130294.56(28)	-0.04
40									
41	31	130444.86(20)	-0.03	130445.18(29)	130449.23(31)	-0.06	130451.76(20)	130458.82(20)	-0.13
42	32	130604.53(28)	-0.22	130606.01(30)	130609.25(20)	-0.11	130613.84(20)	130622.17(21)	2.09
43	33	130761.15(20)	-0.36	130762.44(34)	130765.71(20)	-0.31	130770.15(20)	130776.40(21)	-0.32
44	34	130914.09(22)	-0.01	130914.88(21)	130918.87(32)	0.14	130919.56(20)	130929.14(28)	-0.12
45	35	131060.85(20)	-0.94	131062.55(23)	131066.41(22)	-0.50	131070.92(20)	131071.57(20)	-1.07

103559.594(19) cm^{-1} , measured by Eyler and co-workers [11]. The uncertainty of the $EF^1\Sigma_g^+, \nu'_{EF}=6, J'=0$ term energy is much smaller than that of the measured transition energies and therefore does not contribute significantly to the uncertainties of the $B''\bar{B}^1\Sigma_u^+$ term energies presented here.

Three to eight independent scans in the H^+ detection channel were used to determine average transition energies. The results for states with term energies below the barrier, along with a comparison of the experimental energies with previous measurements, are reported in Table I. Sources of uncertainty include the statistical errors associated with fits to signal and calibration features, calibration transition energy uncertainties, and uncertainty arising from wavelength nonlinearities in the drive of the probe laser. The combined estimate of these uncertainties was similar to the standard deviation observed for a given transition energy measurement obtained from multiple scans. The larger of the two is reported as the uncertainty in Table I. The majority of the observed energies agree with previous results to within the experimental uncertainties reported here and by de Lange *et al.* [6]. Notable exceptions in agreement are the $\nu_{\bar{B}}=32, J=4$ level and the rotational levels of the $\nu_{\bar{B}}=35$ state. In the energy region of the $\nu_{\bar{B}}=35, J=4$ state, de Lange *et al.* observed two transitions, 4a and 4b. In our experiment, only one transition was observed and it matches best the term energy of the 4a state. In Table I, the observed difference is given.

State assignments were aided by comparing the observed term energies with calculated energies obtained by using the program LEVEL, version 7.5, developed by LeRoy [12]. This code uses the Numerov algorithm to integrate the radial Schrödinger equation to determine the energy eigenvalues and eigenfunctions of a given potential energy curve. The latest $B''\bar{B}^1\Sigma_u^+$ adiabatic potential curve and nonadiabatic corrections calculated by Staszewska and Wolniewicz were used [7]. The accuracy of the calculated energies in comparison to the observed energies decreases progressively near and above the barrier. Given that the double-well nature of the $B''\bar{B}^1\Sigma_u^+$ state presents specific challenges for *ab initio* theory, the observed energies reported here can provide an important guide for theoretical work.

The LEVEL code was also used to calculate the vibrational wavefunction overlap between various $EF^1\Sigma_g^+, \nu'_{EF}=6, J'$ levels and the $B''\bar{B}^1\Sigma_u^+, \nu_{B''\bar{B}}, J$ levels to estimate relative signal sizes for different vibrational transitions. These calculations predict that the probe signal should be very weak for inner-well levels, which is consistent with the fact that we did not observe transitions to any inner-well levels. Consequently the inner-well vibrational levels are left blank in Table I. The lowest vibrational level in the outer well we were able to detect was the $\nu_{\bar{B}}=17$ which is also consistent with the calculation because the vibrational wavefunction overlap falls off as one gets deeper in the outer well.

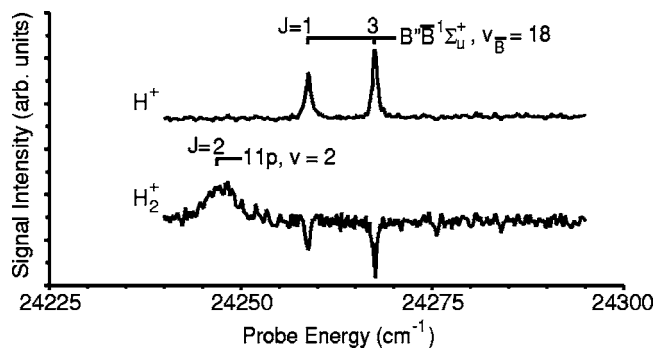


FIG. 3. H^+ and H_2^+ probe spectra in the energy region of the $P(2)$ and $R(2)$ branches of the $B''\bar{B}^1\Sigma_u^+$, $\nu_{B''\bar{B}}=18, J \leftarrow EF^1\Sigma_g^+, \nu'_{EF}=6, J'=2$ transition.

Figure 3 shows an example of the probe spectra in the energy region of the $P(2)$ and $R(2)$ branches to the $B''\bar{B}^1\Sigma_u^+, \nu_{B''\bar{B}}=18$ state located deep in the outer well of the $B''\bar{B}^1\Sigma_u^+$ state. The broad feature observed in the H_2^+ channel corresponds to the $Q(2)$ transition to the $11p, \nu=2$ autoionizing Rydberg level of H_2 . In the H^+ channel transitions to levels of the $B''\bar{B}^1\Sigma_u^+$ state appear as peaks on top of a nonresonant background. Conversely, in the H_2^+ channel these transitions appear as dips in a nonresonant background. This behavior was observed for most outer well levels and it reflects the excitation scheme and decay dynamics of these states. Off resonance, the background continuum in the H_2^+ channel is produced by direct ionization by one-photon absorption of a probe photon. The absorption of another probe photon can then dissociate H_2^+ to create the nonresonant H^+ background. A study of the nonresonant signal strengths as a function of probe pulse energy confirms the one-photon and two-photon nature of these backgrounds, respectively. Bound states excited by one-photon absorption can autoionize, thereby creating H_2^+ , or absorb another photon to create H^+ . The latter process dominates in the excitation of outer well levels of the $B''\bar{B}^1\Sigma_u^+$ state since these levels have negligible autoionization rates due to their poor vibrational wavefunction overlap with the ground state of the ion. This excitation pathway competes with direct ionization and therefore results in a dip in the H_2^+ channel.

The peak and dip signature of the transitions varies for energies near and above the barrier. The degree to which dips or peaks occurs is affected by the relative transition strengths to continua and bound states and the competition between

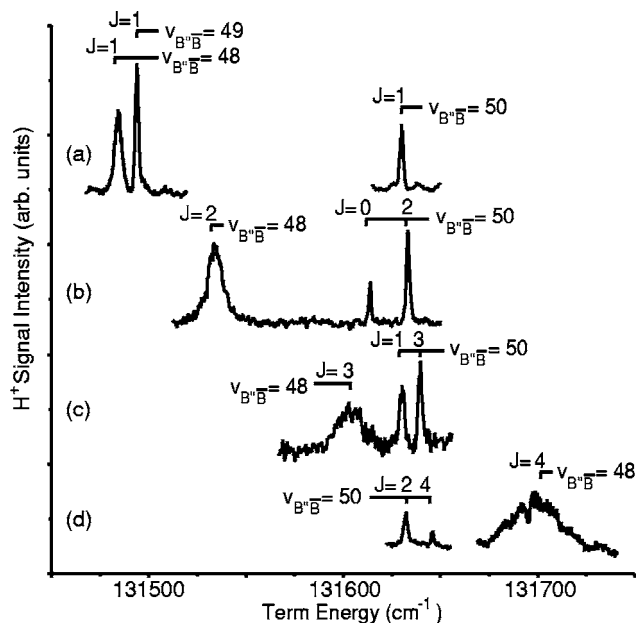


FIG. 4. H^+ probe spectra showing transitions to several levels of the $B''\bar{B}^1\Sigma_u^+$ state in an energy region above the double-well barrier of the $B''\bar{B}^1\Sigma_u^+$ state. The (a)–(d) labels indicate signals obtained via excitation of the $Q(0)$, $Q(1)$, $Q(2)$, and $Q(3)$ $EF^1\Sigma_g^+, \nu'_{EF}=6 \leftarrow X^1\Sigma_g^+, \nu''=0$ pump transitions, respectively.

autoionization and further photoexcitation. A systematic study of this behavior including a careful lineshape analysis are important areas for future investigation to clarify the decay dynamics of these states.

Note that the levels observed are all above the $H(n=1) + H(n=2)$ dissociation limit. For probe light bluer than ~ 366 nm, $H(n=2)$ can be photoionized to yield H^+ . However we see no evidence of the onset of this process in the probe spectra. With our excitation scheme, when on resonance with a transition to a level of the $B''\bar{B}^1\Sigma_u^+$ state, an H^+ signal produced by dissociation followed by ionization of $H(n=2)$ cannot be distinguished from that produced by photoabsorption to the continua of H_2^+ followed by dissociation. As discussed by de Lange *et al.* [6], however, the $B''\bar{B}^1\Sigma_u^+$ state is not expected to dissociate, so we attribute the source of the H^+ signal as being due to the dissociation of H_2^+ .

Figure 4 shows example H^+ probe spectra in the energy region above the barrier obtained by using several pump transitions. Numerous probe transitions are observed in this region which are assigned to levels of the $B''\bar{B}^1\Sigma_u^+$ state. The

TABLE II. Experimental term energies and proposed assignments for observed levels of the $B''\bar{B}^1\Sigma_u^+$ state located above the double-well barrier. Energy values are in cm^{-1} .

$\nu_{B''\bar{B}}$	$J=0$	$J=1$	$J=2$	$J=3$	$J=4$
46	131187.60(37)	131197.95(26)	131207.09(32)	131214.68(25)	131222.28(20)
47	131356.57(25)	131359.43(22)	131365.71(34)	131393.66(23)	131462.27(20)
48		131485.19(66)	131533.16(48)	131604.12(20)	131696(3)
49	131493(1)	131494.15(34)	131498.25(48)	131504.72(56)	131522.22(20)
50	131613.71(74)	131630.45(38)	131632.96(32)	131638.92(35)	131647.03(20)

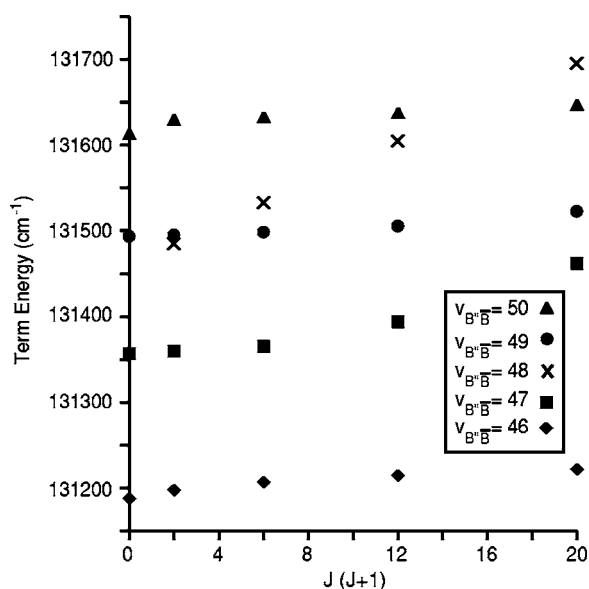


FIG. 5. Experimental term energies as a function of $J(J+1)$ using the proposed assignments given in Table II.

resulting term energies and proposed assignments are reported in Table II. Note that we were not able to make an assignment for the $J=0$ level of the $\nu_{B''\bar{B}}=48$ state. The larger standard deviations observed for some of these data when compared to the energy uncertainties reported in Table I, are due to a less accurate calibration of the probe laser in this energy region.

In Fig. 5 the term energies from Table II are plotted as a function of $J(J+1)$ to display their behavior with rotation. As can be seen in Fig. 5 and in the spectra of Fig. 4 the proposed assignments imply that the $\nu_{B''\bar{B}}=48$ state crosses the $\nu_{B''\bar{B}}=49$ state between $J=1$ and 2 and crosses the $\nu_{B''\bar{B}}=50$ state between $J=3$ and 4. The linear behavior of the energies with $J(J+1)$ shown in Fig. 5 supports this interpretation and indicates that even though these states lie above the barrier, they appear to retain distinguishable inner and outer-well character. The relatively small average rotational constant ($\sim 1.5 \text{ cm}^{-1}$) observed for the $\nu_{B''\bar{B}}=46, 47, 49,$ and 50 levels

and the larger rotational constant ($\sim 11.7 \text{ cm}^{-1}$) for the $\nu_{B''\bar{B}}=48$ level are also consistent with the trend observed for the rotational constants calculated by using the LEVEL program of the outer and inner-well levels below the barrier, respectively. Finally, note in Fig. 4 the relatively large and increasing linewidth with J of the $\nu_{B''\bar{B}}=48$ level, which is not observed for the neighboring $\nu_{B''\bar{B}}=50$ level. It would be not surprising if the $\nu_{B''\bar{B}}=48$ level with its inner-well character had a larger autoionization rate than the other levels with predominant outer-well character since its wave function overlap with the ground state of the ion should be relatively enhanced. Further investigation, however, will be needed to definitively attribute this broadening to the onset of autoionization.

IV. CONCLUSIONS

Double resonance spectroscopy via the four lowest rotational levels of the $EF^1\Sigma_g^+, \nu_{EF}=6$ state has been used to probe the rovibrational structure of the *ungerade* double-well $B''\bar{B}^1\Sigma_u^+$ state. The energies of many rovibronic levels of the $B''\bar{B}^1\Sigma_u^+$ state are reported. The energy measurements at and above the double-well barrier may be useful for improving the accuracy of the potential energy curve for the $B''\bar{B}^1\Sigma_u^+$ state. Based on the observations reported here, future work to investigate energy levels above $\nu_{B''\bar{B}}=50$ and approaching the $H(n=3)$ dissociation threshold should be possible. In addition, evidence of varying state dynamics in the energy region above the barrier has been observed. An investigation of the lineshapes of the transitions to the $B''\bar{B}^1\Sigma_u^+$ state as a function of vibrational quantum number in both the H^+ and H_2^+ channels therefore holds promise for understanding its decay processes.

ACKNOWLEDGMENTS

This work was supported by a grant from the National Science Foundation Grant No. (PHY-0140296). A.M. would like to acknowledge postdoctoral support from the Keck Foundation. We would also like to thank R. J. LeRoy for providing us with the LEVEL program.

-
- [1] S. Ross and Ch. Jungen, *Phys. Rev. Lett.* **59**, 1297 (1987).
 [2] S. Yu and K. Dressler, *J. Chem. Phys.* **101**, 7692 (1994).
 [3] E. Reinhold, W. Hogervorst, W. Ubachs, and L. Wolniewicz, *Phys. Rev. A* **60**, 1258 (1999).
 [4] I. Dabrowski and G. Herzberg, *Can. J. Phys.* **52**, 1110 (1974).
 [5] W. Kolos, *J. Mol. Spectrosc.* **62**, 429 (1976).
 [6] A. de Lange, W. Hogervorst, W. Ubachs, and L. Wolniewicz, *Phys. Rev. Lett.* **86**, 2988 (2001).
 [7] G. Staszewska and L. Wolniewicz, *J. Mol. Spectrosc.* **212**, 208 (2002); <http://www.phys.uni.torun.pl/ftp/publications/ifiz/luwo/1Su.02>; http://www.phys.uni.torun.pl/ftp/publications/ifiz/luwo/EF_e_h98
 [8] B. A. Palmer, R. A. Keller, and R. Engleman, <http://www.lac.u-psud.fr/Database/Tab-long/UI-Wv.html>
 [9] F. M. Phelps III, *M.I.T. Wavelength Tables* (MIT Press, Cambridge, MA, 1982).
 [10] G. H. Dieke, *J. Mol. Spectrosc.* **2**, 494 (1958).
 [11] Y. P. Zhang, C. L. Gan, J. P. Song, X. J. Yu, H. Ge, R. Q. Ma, C. S. Li, K. Q. Lu, and E. E. Eyler, *Chin. Phys. Lett.* **22**, 1110 (2005); J. M. Gilligan and E. E. Eyler, *Phys. Rev. A* **46**, 3676 (1992).
 [12] R. J. LeRoy, "LEVEL 7.5, A computer program for solving the radial Schrödinger equation for bound and quasibound levels," University of Waterloo, Chemical Physics Research Report No. CP-655, 2002, <http://leroy.uwaterloo.ca>